ORGANOMETALLICS

ARTICLE

pubs.acs.org/Organometallics

Tetrapalladium(II) Bisazobenzene and Azoazoxybenzene Complexes: Syntheses, Electronic Structures, and Optical Properties

Octavia A. Blackburn, Benjamin J. Coe,* and Madeleine Helliwell

School of Chemistry, University of Manchester, Oxford Road, Manchester M13 9PL, U.K.

Supporting Information

ABSTRACT: Three new tetranuclear, chloride-bridged Pd^{II} complexes have been prepared by using 1,4-bis[(*E*)-phenylazo]benzenes (BPABs) and an azoazoxybenzene derivative. The latter was obtained unexpectedly by reacting *N*,*N*-dimethyl-4-nitrosoaniline with 2,3,5,6-tetramethylphenylenediamine in glacial acetic acid. Characterization includes ^{1}H NMR and UV−vis spectroscopies, and single-crystal X-ray structures have been obtained for two of the proligands and one complex. As expected, the methyl groups on the central aryl rings cause severe departures from planarity. The proligands show an intense UV absorption ($\lambda_{max} \approx 350$ nm) due to $\pi \rightarrow \pi^*$ intramolecular charge transfer, together with weaker n $\rightarrow \pi^*$ bands in the visible region. The complexes display an intense visible band ($\lambda_{max} = 449-475$ nm) and multiple near-UV absorptions. While the electronic absorption spectra of the BPAB complexes are quite similar, the azoazoxybenzene complex shows a doubly intense visible band. Dichroic ratios (DRs) measured in two different liquid crystal (LC) hosts show that complexation is not beneficial, as noted for dinuclear azobenzene complexes previously. The shape of the new complexes appears to give relatively poor alignment within the LC. Time-dependent density functional theory reveals differing origins of the low-energy transitions for BPAB and azoazoxybenzene complexes, those for the latter involving charge transfer within the N═N(O)$C_6H_3NMe_2$ moieties. The origin of the low-energy transition of the BPAB complex also differs from that in the related dinuclear complexes. The directions of the μ_{12} vectors calculated with respect to the long molecular axis generally correlate with the observed DR values, with better alignment for the low-energy transitions that are relatively more dichroic.

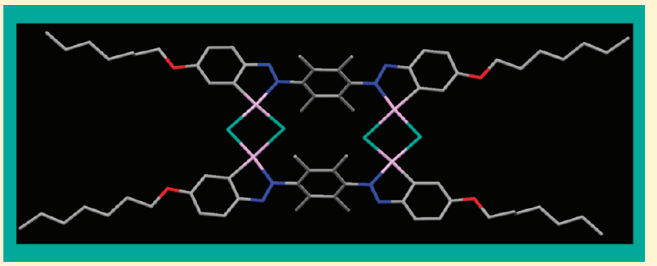

INTRODUCTION

Palladacyclic complexes have relevance to many emerging applications involving for example catalysis,[1] nonlinear optics,[2] or liquid crystalline materials.[3] We described recently studies with dinuclear cyclopalladated azobenzenes (e.g., **1**−**4**, Figure 1),[4] as part of our work on the dichroic properties of metal complexes, a relatively unexplored area.[5] In this context, we have studied also Ni^{II} and Pd^{II} complexes of linearly connected azobenzene ligands.[6] Dichroic dyes show orientation-dependent absorption intensities and are of interest for potential use in guest−host liquid crystal displays (GH-LCDs). In a GH-LCD, an applied electric field is used to manipulate the orientation of the molecules and thus change the appearance of the display.[7] This technology has promise for applications such as electronic paper.[8] The dichroic ratio (DR) is the ratio of the absorbances when illuminated by light polarized parallel ($A_{||}$) and perpendicular ($A_{\perp}$) to the liquid crystal (LC) director. DR values large enough for commercial use require the dye molecules to be well aligned in the LC matrix, with the transition dipole moment (μ_{12}) of the color-inducing electronic transition(s) coinciding with the long molecular axis.

In this article, we describe the synthesis and properties of tetranuclear Pd^{II} complexes that incorporate bisazobenzene or azoazoxybenzene ligands to create a rectangular motif. While dinuclear cyclopalladated azobenzenes are well-known, to our knowledge cyclopalladation of bisazobenzenes or azoazoxybenzenes is unprecedented. In order to obtain the desired motif, palladation of the central aryl rings is prevented by methyl

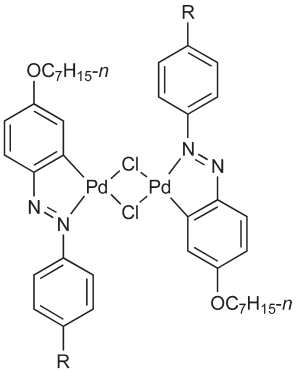

R = NO_2 (**1**), CN (**2**), F (**3**), CO_2Et (**4**)

Figure 1. Dominant isomeric structures of the chloride-bridged dipalladium(II) complexes studied previously.[4]

Received: June 3, 2011
Published: August 30, 2011

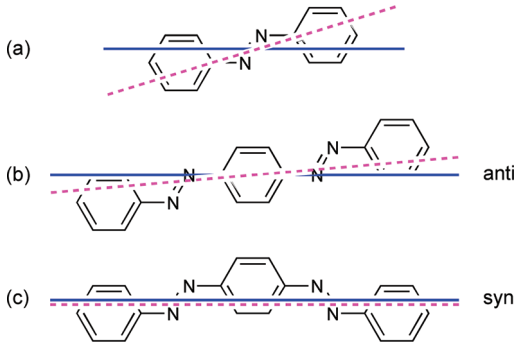

Figure 2. The structures of (*E*)-azobenzene (a) and BPAB in its anti (b) and syn (c) conformations, showing the approximate μ_{12} vectors (pink dashed lines). The solid blue lines represent the long molecular axes.

substituents. Related tetranuclear complexes of diimine ligands have been investigated previously for their liquid crystalline properties.[9,10]

Azobenzenes are commonly used as dichroic dyes owing to their long slender shape and the relatively close alignment of μ_{12} for the intense $\pi \rightarrow \pi^*$ intramolecular charge-transfer (ICT) transition with the long molecular axis. Given that the DRs of bisazobenzenes exceed those of azobenzenes,[11] we anticipated that the new tetrapalladium complexes might outperform their dinuclear counterparts studied previously. Furthermore, the angle between the μ_{12} vector and the long molecular axis for a 1,4-bis[(*E*)-phenylazo]benzene (BPAB) in its anti conformation (Figure 2) has been calculated to be 4.38°,[12] compared to 17° for (*E*)-azobenzene.[13] In the tetrapalladated structures described here, the ligands are forced to adopt a syn arrangement, in which the μ_{12} vector coincides exactly with the long molecular axis.

EXPERIMENTAL SECTION

Materials and Procedures. The complex $PdCl_2(NCPh)_2$[14] was synthesized by published methods. All other chemicals were used as supplied by Sigma Aldrich or Alfa Aesar, and the LCs used for dichroism measurements were supplied by Merck and Synthon. Products were dried at room temperature overnight in a vacuum desiccator ($CaSO_4$) or by direct attachment to a high-vacuum line for several hours prior to characterization.

General Physical Measurements. ^{1}H NMR spectra were recorded on Bruker UltraShield 500 or AV 400 spectrometers, and all shifts are quoted with respect to TMS. The fine splitting of phenyl ring AA′BB′ patterns is ignored, and the signals are reported as simple "doublets", with "*J* values" (in Hz) referring to the two most intense peaks. Electrospray mass spectrometry was performed on a Micromass Platform II, and MALDI mass spectra were recorded on a Shimadzu Axima Confidence instrument with dichloromethane as the solvent. In cases where clusters of peaks are observed due to the presence of various isotopes, the most intense peak is always quoted. Elemental analyses were performed by the Microanalytical Laboratory, University of Manchester. UV−vis spectra were obtained by using a Shimadzu UV-2401 PC spectrometer. Dichroism measurements were performed on a custom-built Hewlett-Packard machine supplied by HP Research (U.K.). Abbreviations: br = broad; s = singlet; d = doublet; dd = doublet of doublets; t = triplet; q = quartet; qnt = quintet.

Synthesis of 1,4-Bis[4-*n*-heptoxy-(*E*)-phenylazo]-2,3,5,6-tetramethylbenzene ($6H_2$). To a stirred solution of 2,3,5,6-tetramethylphenylenediamine (TMPD, 1.00 g, 6.09 mmol) in hydrochloric acid (37%, 4 mL) cooled in an ice bath to below 5 °C was added dropwise a solution of $NaNO_2$ (0.92 g, 13.3 mmol) in water (10 mL). The solution was stirred at 0−5 °C for 1 h. This orange diazonium salt solution was then added slowly to a cooled solution of phenol (1.15 g, 12.2 mmol) and NaOH (1.12 g, 28.0 mmol) in water (20 mL), maintained below 5 °C for the duration of the addition. The resulting suspension was stirred with cooling for 1 h, then allowed to warm to room temperature and stirred for a further 1 h. The suspension was filtered to remove a dark brown precipitate, and the filtrate was acidified to pH 5 by using 1 M HCl. The resulting orange precipitate was filtered off, and crude **5** obtained by silica gel column chromatography eluting with 92:8 dichloromethane/ethyl acetate (yield 80 mg): δ_H (400 MHz, CD_3COCD_3) 9.12 (2 H, br, OH), 7.86 (4 H, d, *J* = 8.9, *B*), 7.05 (4 H, d, *J* = 8.9, *A*), 2.12 (12 H, s, 4Me); *m*/*z* (−ES) 373 ($[M - H]^-$). This material was combined with 1-bromoheptane (84 mg, 0.469 mmol) and K_2CO_3 (118 mg, 0.854 mmol) in DMF (10 mL), and the mixture heated under reflux for 3 h. The resulting solution was poured into cold water, and the precipitate was filtered off and recrystallized from ethanol to give an orange solid (70 mg, 2%): δ_H (400 MHz, $CDCl_3$) 7.92 (4 H, d, *J* = 8.9, *B*), 7.03 (4 H, d, *J* = 8.9, *A*), 4.05 (4 H, t, *J* = 6.6, $2OCH_2$), 2.12 (12 H, s, 4Me), 1.83 (4 H, qnt, *J* = 6.5, $2CH_2$), 1.52−1.28 (16 H, $8CH_2$), 0.90 (6 H, t, *J* = 6.7, 2Me); *m*/*z* (+ES) 571 ($[M + H]^+$). Anal. Calcd (%) for $C_{36}H_{50}N_4O_2$: C, 75.8; H, 8.8; N, 9.8. Found: C, 75.6; H, 9.0; N, 9.8. Diffraction-quality crystals were grown by layering hexane on top of a dichloromethane solution.

Synthesis of 1-Amino-4-[4-(ethoxycarbonyl)-(*E*)-phenylazo]-2,3,5,6-tetramethylbenzene (9). To a stirred solution of ethyl-4-aminobenzoate (1.50 g, 9.08 mmol) in dichloromethane (30 mL) was added a solution of oxone (11.20 g, 18.2 mmol) in water (120 mL). The mixture was stirred under argon for 1 h, and the organic phase acquired a green color. The layers were separated, and the aqueous phase washed with dichloromethane (2 × 20 mL). The combined organic layers were washed with 1 M HCl (2 × 50 mL), saturated aqueous $NaHCO_3$ (2 × 50 mL), and water (2 × 50 mL), then dried over $MgSO_4$ and evaporated to give crude **8** as a pale yellow solid (1.27 g): δ_H (400 MHz, $CDCl_3$) 8.30 (2 H, d, *J* = 8.8, C_6H_4), 7.93 (2 H, d, *J* = 8.8, C_6H_4), 4.43 (2 H, q, *J* = 7.1, CH_2), 1.43 (3 H, t, *J* = 7.1, Me); *m*/*z* (−ES) 180 ($[M + H]^-$). This material was used without further purification due to limited stability; it was combined with TMPD (1.16 g, 7.06 mmol) in toluene (50 mL) and glacial acetic acid (2 mL) and heated at reflux for 24 h. After cooling to room temperature, the dark red solution was washed with water (3 × 50 mL), dried over $MgSO_4$, and evaporated to dryness. Purification was achieved by silica gel column chromatography eluting with dichloromethane to yield a dark red solid (465 mg, 16%): δ_H (400 MHz, $CDCl_3$) 8.17 (2 H, d, *J* = 8.5, *D*), 7.87 (2 H, d, *J* = 8.5, *C*), 4.42 (2 H, q, *J* = 7.1, CH_2), 3.93 (2 H, s, NH_2), 2.38 (6 H, s, 2Me), 2.17 (6 H, s, 2Me), 1.43 (3 H, t, *J* = 7.1, CO_2CH_2Me): *m*/*z* (+ES) 326 ($[M + H]^+$), 348 ($[M + Na]^+$). Anal. Calcd (%) for $C_{19}H_{23}N_3O_2$: C, 70.1; H, 7.1; N, 12.9. Found: C, 69.9; H, 7.1; N, 12.8.

Synthesis of 1-[4-(Ethoxycarbonyl)-(*E*)-phenylazo]-4-[4-*n*-heptoxy-(*E*)-phenylazo]-2,3,5,6-tetramethylbenzene ($11H_2$). **9** (130 mg, 0.399 mmol) was dissolved in glacial acetic acid (15 mL) and propionic acid (2.4 mL) and cooled to below 5 °C in an ice bath. Nitrosyl sulfuric acid (40 wt % solution in sulfuric acid, 140 mg, 0.441 mmol) was added slowly to the stirred dark red solution at 0−5 °C, and stirring was continued for 1 h. This diazonium salt solution was then added slowly to a cooled solution of phenol (41 mg, 0.436 mmol) and NaOH (48 mg, 1.20 mmol) in water (15 mL). The pH was maintained above 7 by adding 2 M aqueous NaOH, and the temperature kept below 5 °C during the addition. The red suspension was stirred for 1 h with cooling, then allowed to warm to room temperature and stirred for a further 1 h. The solid was filtered off and purified by silica gel column chromatography eluting with dichloromethane/ethyl acetate (99:1), followed by recrystallization from ethanol to give **10** as a red solid (30 mg): δ_H

Table 1. Crystallographic Data and Refinement Details for the Proligands $6H_2$ and $15H_2$ and Complex 7

	$6H_2$	$15H_2$	7
formula	$C_{36}H_{50}N_4O_2$	$C_{31}H_{41}N_5O_2$	$C_{73}H_{98}Cl_6N_8O_4Pd_4$
M	570.80	515.69	1789.89
cryst syst	triclinic	triclinic	triclinic
space group	$P\bar{1}$	$P\bar{1}$	$P\bar{1}$
a/Å	5.4082(9)	5.6665(9)	10.730(3)
b/Å	9.1179(15)	9.3701(14)	11.944(3)
c/Å	16.912(3)	27.180(4)	16.333(4)
α/deg	98.067(3)	82.750(3)	97.487(4)
β/deg	96.340(3)	87.528(3)	94.532(4)
γ/deg	102.416(3)	75.106(3)	115.473(4)
U/Å^3	797.8(2)	1383.4(4)	1852.2(8)
Z	1	2	1
T/K	100(2)	100(2)	100(2)
μ/mm^{-1}	0.074	0.079	1.225
cryst size/mm	0.60 × 0.50 × 0.20	0.60 × 0.60 × 0.02	0.30 × 0.25 × 0.10
appearance	orange plate	yellow plate	yellow plate
no. of reflns collected	4696	8641	14 280
no. of indep reflns (R_{int})	3194 (0.0355)	3978 (0.0843)	7395 (0.0293)
reflns with $I > 2\sigma(I)$	2310	1891	5855
goodness-of-fit on F^2	0.981	0.777	1.105
final R_1, wR_2 [$I > 2\sigma(I)$]	0.0457, 0.1045	0.0436, 0.0639	0.0485, 0.0991
(all data)	0.0688, 0.1291	0.1197, 0.0796	0.0679, 0.1060
peak and hole/e Å^{-3}	0.274, −0.285	0.166, −0.148	0.987, −0.877

(500 MHz, $CDCl_3$) 8.23 (2 H, d, J = 8.7, *D*), 7.96 (2 H, d, J = 8.7, *C*), 7.89 (2 H, d, J = 8.8, *B*), 6.96 (2 H, d, J = 8.8, *A*), 5.53 (1 H, br, OH), 4.44 (2 H, q, J = 7.1, CH_2), 2.19 (6 H, s, 2Me), 2.12 (6 H, s, 2Me), 1.44 (3 H, t, J = 7.1, CO_2CH_2*Me*); m/z (+ES) 431 ($[M+H]^+$); m/z (−ES) 429 ($[M-H]^-$). This compound (90 mg) was reacted with 1-bromoheptane (45 mg, 0.251 mmol) and K_2CO_3 (58 mg, 0.420 mmol) in DMF (10 mL) in a manner identical to **$6H_2$**. The product was purified by recrystallization from hexane/ethanol to give an orange-red solid (36 mg, 6%): δ_H (400 MHz, $CDCl_3$) 8.23 (2 H, d, J = 8.8, *D*), 7.97−7.90 (4 H, *B* + *C*), 7.04 (2 H, d, J = 9.1, *A*), 4.43 (2 H, q, J = 7.1, CO_2CH_2), 4.06 (2 H, t, J = 6.6, OCH_2), 2.20 (6 H, s, 2Me), 2.12 (6 H, s, 2Me), 1.84 (2 H, qnt, J = 6.7, CH_2), 1.53−1.29 (11 H, C_4H_8 + CO_2CH_2*Me*), 0.91 (3 H, t, J = 7.0, Me); m/z (+ES) 529 ($[M+H]^+$), 551 ($[M+Na]^+$). Anal. Calcd (%) for $C_{32}H_{40}N_4O_3$: C, 72.7; H, 7.6; N, 10.6. Found: C, 72.5; H, 7.5; N, 10.3.

Synthesis of 1-Amino-4-[4-(dimethylamino)-(*E*)-phenyl-*ONN*-azoxy]-2,3,5,6-tetramethylbenzene (13). *N*,*N*-Dimethyl-4-nitrosoaniline (1.00 g, 6.66 mmol) and TMPD (1.09 g, 6.64 mmol) were combined in glacial acetic acid (100 mL) and stirred under a flow of argon for 24 h. The dark green solution was diluted with water (100 mL), and the product extracted with dichloromethane (3 × 50 mL). The combined organic extracts were washed with water (2 × 100 mL), dried over $MgSO_4$, and evaporated to give a dark khaki solid. Purification was achieved by recrystallization from ethanol/dichloromethane to yield a gold-colored solid, and further crops were obtained by subsequent recrystallizations of the filtrate (1.19 g, 57%): δ_H (400 MHz, $CDCl_3$) 8.23 (2 H, d, J = 9.4, *C*), 6.68 (2 H, d, J = 9.4, *D*), 3.58 (2 H, br, NH_2), 3.07 (6 H, s, NMe_2), 2.11 (6 H, s, 2Me), 2.00 (6 H, s, 2Me); m/z (+ES) 313 ($[M+H]^+$). Anal. Calcd (%) for $C_{18}H_{24}N_4O$: C, 69.2; H, 7.7; N, 17.9. Found: C, 69.0; H, 7.8; N, 17.6.

Synthesis of 1-[4-(Dimethylamino)-(*E*)-phenyl-*ONN*-azoxy]-4-(4-*n*-heptoxyphenylazo)-2,3,5,6-tetramethylbenzene ($15H_2$). Precursor **14** was prepared in a manner identical to **5**. Addition of $NaNO_2$ (0.26 g, 3.77 mmol) to **13** (1.00 g, 3.20 mmol) in concentrated HCl (37%, 1.0 mL) and water (20 mL) gave a dark yellow-green solution. Coupling with phenol (0.32 g, 3.40 mmol) in 1 M aqueous NaOH (7.8 mL) produced a yellow-brown precipitate. Recrystallization from dichloromethane/ethanol gave **14** as a yellow solid (250 mg): δ_H (400 MHz, CD_3SOCD_3) 8.14 (2 H, d, J = 9.3, *C*), 7.77 (2 H, d, J = 8.8, *B*), 6.96 (2 H, d, J = 8.8, *A*), 6.81 (2 H, d, J = 9.4, *D*), 3.05 (6 H, s, NMe_2), 2.04 (6 H, s, 2Me), 1.92 (6 H, s, 2Me); m/z (+ES) 418 ($[M+H]^+$), 440 ($[M+Na]^+$); m/z (−ES) 416 ($[M-H]^-$). This compound (200 mg) was reacted with 1-bromoheptane (107 mg, 0.597 mmol) and K_2CO_3 (137 mg, 0.991 mmol) in DMF (15 mL) in a manner identical to **$6H_2$**. The crude product was recrystallized from dichloromethane/ethanol to give an orange solid (175 mg, 13%): δ_H (400 MHz, $CDCl_3$) 8.26 (2 H, d, J = 9.3, *C*), 7.91 (2 H, d, J = 9.0, *B*), 7.02 (2 H, d, J = 9.0, *A*), 6.71 (2 H, d, J = 9.4, *D*), 4.05 (2 H, t, J = 6.5, OCH_2), 3.09 (6 H, s, NMe_2), 2.12 (6 H, s, 2Me), 2.03 (6 H, s, 2Me), 1.84 (2 H, qnt, J = 6.7, CH_2), 1.53−1.25 (8 H, C_4H_8), 0.91 (3 H, t, J = 7.0, Me); m/z (+ES) 517 ($[M+H]^+$), 539 ($[M+Na]^+$). Anal. Calcd (%) for $C_{31}H_{41}N_5O_2$: C, 72.2; H, 8.0; N, 13.6. Found: C, 72.1; H, 8.3; N, 13.6. Diffraction-quality crystals were grown by slow evaporation of a dichloromethane solution.

Synthesis of Tetra(μ-chloro)bis{μ-[2,3,5,6-tetramethyl-1,4-phenylenebis[(*E*)-azo-4-(*n*-heptoxy)-1,2-phenylene]]}tetrapalladium, $Pd_4(\mu\text{-}Cl)_4(6)_2$ (7). **$6H_2$** (30 mg, 0.053 mmol) and $PdCl_2(NCPh)_2$ (45 mg, 0.117 mmol) were combined in ethanol (20 mL), and the mixture was heated under reflux for 8 h. After cooling, the ochre precipitate was filtered off and washed with a small amount of ethanol (yield 35 mg, 77%): δ_H (400 MHz, $CDCl_3$) 7.77 (4 H, d, J = 8.6, *c*), 6.95 (4 H, d, J = 2.5, *a*), 6.74 (4 H, dd, J_{bc} = 8.4, J_{ab} = 2.5, *b*), 4.12 (8 H, t, J = 6.4, $4OCH_2$), 2.21 (24 H, s, 8Me), 1.85 (8 H, qnt, J = 6.7, $4CH_2$), 1.54−1.28 (32 H, $4C_4H_8$), 0.91 (12 H, t, J = 7.2, 4Me); m/z (+MALDI) 1668 ($[M-Cl]^+$), 1729 ($[M+Na]^+$). Anal. Calcd (%) for $C_{72}H_{96}Cl_4N_8O_4Pd_4$: C, 50.7; H, 5.7; N, 6.6. Found: C, 50.7; H, 5.7; N, 6.5. Diffraction-quality crystals were grown by layering ethanol on top of a dichloromethane solution.

Scheme 1. Syntheses of Bisazobenzene Proligands and Their Chloride-Bridged Tetrapalladium(II) Complexes, Showing the Possible Structural Isomers and ^{1}H NMR Labels[a]

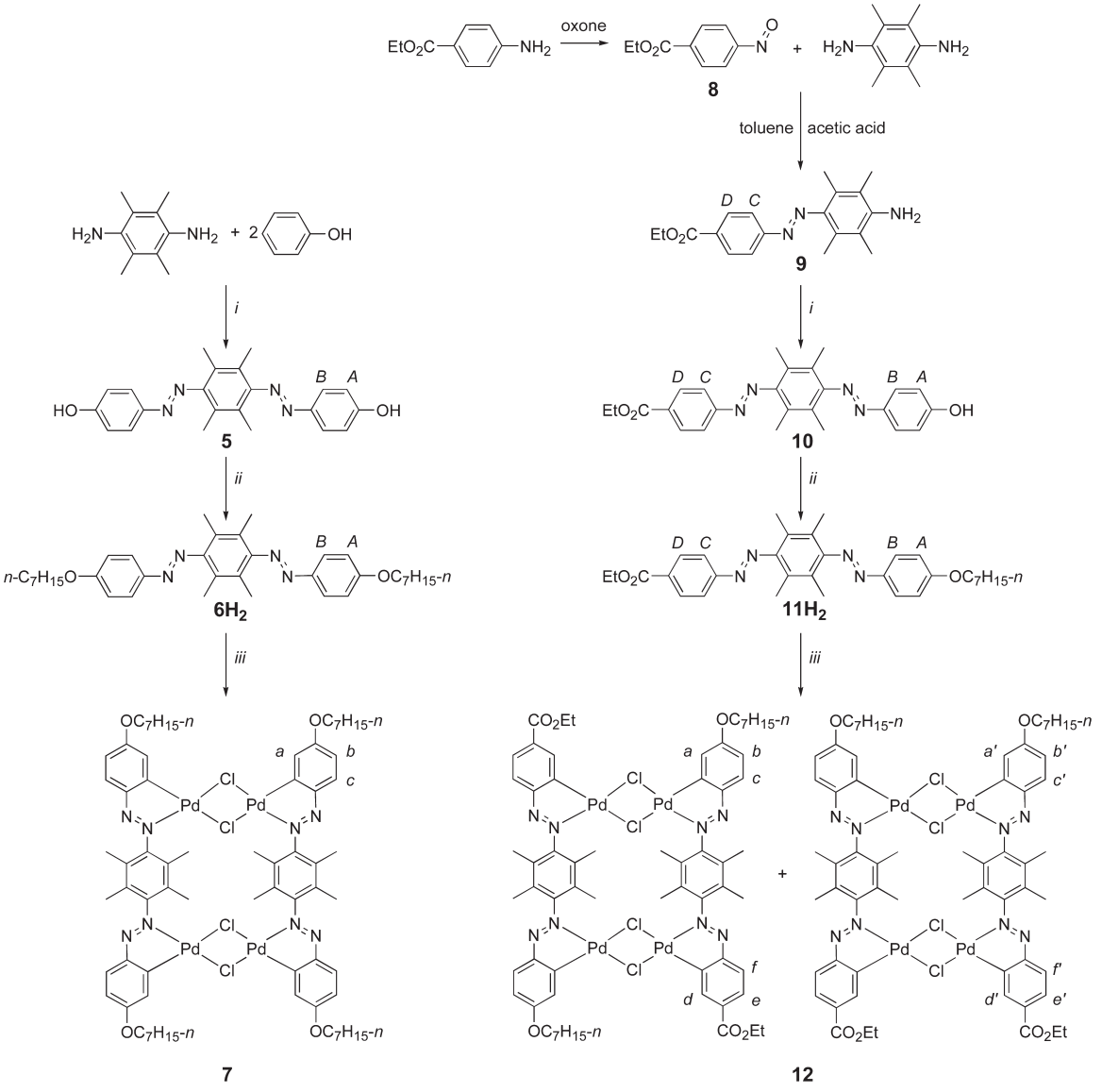

[a] Reagents and solvents: (i) $NaNO_2$/HCl then NaOH/phenol; (ii) *n*-$C_7H_{15}Br/K_2CO_3$/DMF; (iii) $PdCl_2(NCPh)_2$ in ethanol under reflux.

Synthesis of Tetra(*μ*-chloro)bis{*μ*-[2,3,5,6-tetramethyl-1-[(*E*)-azo-4-(*n*-heptoxy)-1,2-phenylene]-4-[(*E*)-azo-4-(ethoxycarbonyl)-1,2-phenylene]phenylene]}tetrapalladium, $Pd_4(\mu\text{-Cl})_4(11)_2$ (12). This compound was prepared in a manner identical to **7** by using $\mathbf{11H_2}$ (30 mg, 0.057 mmol) and $PdCl_2(NCPh)_2$ (44 mg, 0.115 mmol). Purification by recrystallization from dichloromethane/ethanol and washing with diethyl ether gave a yellow solid (32 mg, 69%). ^{1}H NMR spectroscopy reveals a ca. 1:1 mixture of isomers with very closely overlapped signals: δ_H (400 MHz, $CDCl_3$) 8.15−8.12 (4 H, 2s, *d* + *d*′), 8.00−7.94 (8 H, *e* + *e*′, *f* + *f*′), 7.80−7.76 (4 H, 2d, *c* + *c*′), 7.00−6.95 (4 H, 2d, *a* + *a*′), 6.77−6.73 (4 H, 2dd, *b* + *b*′), 4.49−4.41 (8 H, $4CO_2CH_2$), 4.17−4.09 (8 H, $4OCH_2$), 2.23 (24 H, s, 8Me), 2.21 (24 H, s, 8Me), 1.85 (8 H, qnt, *J* = 7.1, $4CH_2$), 1.54−1.30 (44 H, $4C_4H_8$ + $4CO_2CH_2Me$), 0.92 (12 H, t, *J* = 6.8, 4Me); *m*/*z* (+MALDI) 1586 ([M − Cl]$^+$), 1644 ([M + Na]$^+$). Anal. Calcd (%) for $C_{64}H_{76}Cl_4N_8O_6Pd_4$: C, 47.4; H, 4.7; N, 6.9. Found: C, 47.8; H, 4.7; N, 6.7.

Synthesis of Tetra(*μ*-chloro)bis{*μ*-[2,3,5,6-tetramethyl-1-[(*E*)-*ONN*-azoxy-4-(dimethylamino)-1,2-phenylene]-4-[(*E*)-azo-4-(*n*-heptoxy)-1,2-phenylene]phenylene]}tetrapalladium, $Pd_4(\mu\text{-Cl})_4(15)_2$ (16). This compound was prepared in a manner identical to **7** by using $\mathbf{15H_2}$ (40 mg, 0.078 mmol) and $PdCl_2(NCPh)_2$ (68 mg, 0.177 mmol). The product was purified by filtration of a dichloromethane solution through Celite, followed by evaporation of the solvent to yield an orange solid (35 mg, 56%). ^{1}H NMR spectroscopy reveals a dominant isomer with ca. 20% of a minor isomer. Major isomer: δ_H (400 MHz, $CDCl_3$) 7.80 (2 H, d, *J* = 8.6, *c*), 7.36 (2 H, d, *J* = 9.1, *f*′), 6.96 (2 H, d, *J* = 2.5, *a*), 6.77−6.73 (4 H, *b* + *d*), 6.44 (2 H, dd, J_{ef} = 10.0, J_{ed} = 2.5, *e*), 4.10 (4 H, t, *J* = 6.6, $2OCH_2$), 3.16 (12 H, s, NMe_2), 2.20 (12 H, s, 4Me), 2.17 (12 H, s, 4Me), 1.84 (4 H, qnt, *J* = 6.7, $2CH_2$), 1.52−1.29 (16 H, $2C_4H_8$), 0.91 (6 H, t, *J* = 6.9, 2Me); *m*/*z* (+MALDI) 1560 ([M − Cl]$^+$), 1596 ([M + H]$^+$), 1619 ([M + H + Na]$^+$), 1633 ([M + K]$^+$). Anal. Calcd (%) for $C_{62}H_{78}Cl_4N_{10}O_4Pd_4$: C, 46.7; H, 4.9; N, 8.8. Found: C, 46.4; H, 5.3; N, 8.3.

dx.doi.org/10.1021/om200479g |*Organometallics* 2011, 30, 4910–4923

Scheme 2. Synthesis of the Azoazoxybenzene Proligand $15H_2$ and Its Chloride-Bridged Tetrapalladium(II) Complex, Showing the Possible Structural Isomers and ^{1}H NMR Labels[a]

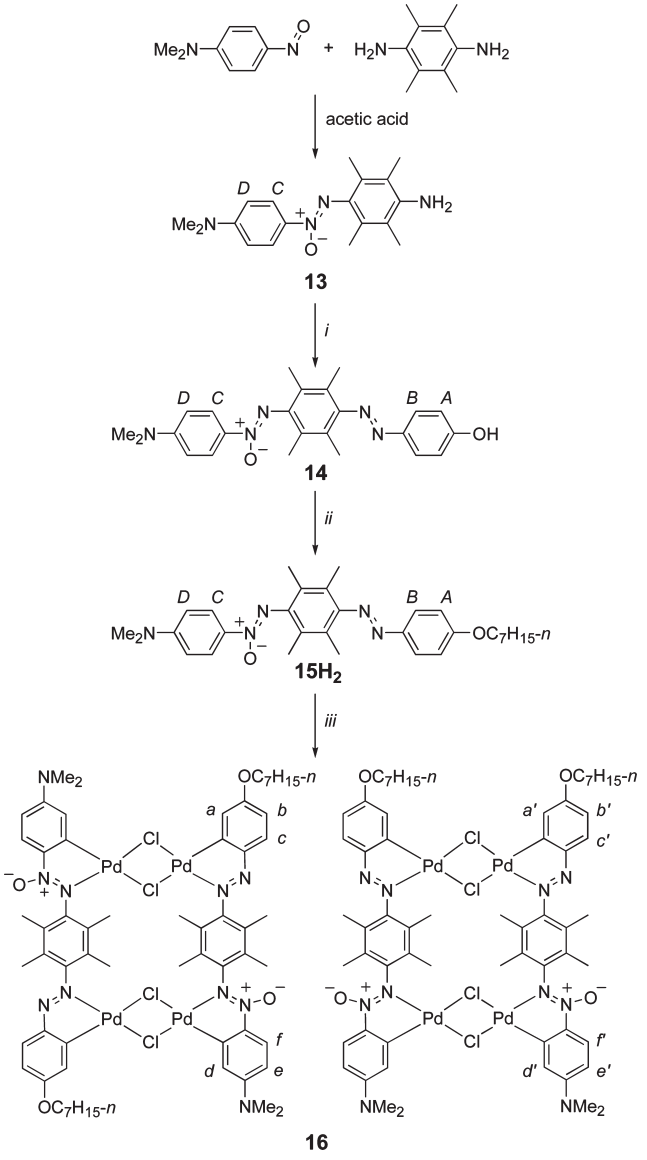

[a] The reagents and reaction conditions (i)−(iii) are as in Scheme 1.

X-ray Crystallography. Crystal structures of the proligands $6H_2$ and $15H_2$ and of the complex **7** have been obtained. Data were collected on a Bruker APEX CCD X-ray diffractometer by using Mo Kα radiation (λ = 0.71073 Å), and the data were processed by using the Bruker SAINT[15] and SADABS[16] software packages. The structures were solved by direct methods by using SHELXS-97[17] and refined by full-matrix least-squares on all F_o^2 data by using SHELXL-97.[18] With the exception of **7**, all non-hydrogen atoms were refined anisotropically, and hydrogen atoms were included in idealized positions by using the riding model, with thermal parameters of 1.2 times those of aromatic parent carbon atoms and 1.5 times those of methyl parent carbons. For $6H_2$, there is half a molecule in the asymmetric unit, with the other half generated by inversion. For $15H_2$, the data were cut at 0.9 Å resolution because the crystal diffracted rather weakly at high angle. The atoms C27−C31 of the C_7H_{15} group are disordered over two semioccupied sites. For **7**, there is half a Pd complex and half a molecule of dichloromethane in the asymmetric unit. The atom Cl2 is disordered over two sites, with occupancies of 60(2):40(2), and the C_6Me_4 group is also disordered over two sites, with occupancies of 55(1):45(1). Therefore, for the disordered atoms Cl2 and Cl2A ISOR was used to reduce ellipsoid elongation and thus prevent the adjacent ellipsoids from encroaching on each other's space. Also, the atoms of the C_6Me_4 unit (C1−C10) were refined isotropically because of the near coincidence of some of them. Crystallographic data and refinement details are presented in Table 1.

Dichroic Ratio Measurements. DR values were measured by using proprietary equipment and software courtesy of Hewlett-Packard Ltd. LC cells were purchased from Linkam Scientific, and syringe filters were purchased from Fisher Scientific UK Ltd. A dye (ca. 1 wt %) was dissolved in the LC by stirring above the clearing temperature for ca. 16 h. Slow cooling was followed by filtration through a PTFE syringe filter of pore size 0.2 μm to remove any undissolved dye. Glass cells, with a 5 μm wide gap and rubbed polyimide surface to give antiparallel alignment, were filled by capillary action above the clearing temperature of the LC and allowed to cool. The absorption of the solution was measured parallel and perpendicular to the direction of rubbing by using polarized light and 90° rotation of the cell. The DR ($A_\perp/A_\parallel$) was calculated at the absorption maximum, except when this lies below the low wavelength limit of the spectrometer (380 nm). A cell containing only the LC was used as a reference, and the quoted DR values are averages from at least two separate measurements. The error on each value is approximated to be a maximum of ±10%, as determined from repeated measurements with a standard black dye (Merck).

Theoretical Studies. Structure optimization (B3LYP/Def2-SVP/SDD)[19−21] and time-dependent density functional theory (TD-DFT) calculations were conducted on models of complexes **7** and **16** (denoted **7′** and **16′**) by using the Gaussian 03 suite of programs.[22] The first 80 excited states were calculated by using the B3LYP exchange−correlation functional and Def-2 SVP/SDD basis sets with inclusion of a COSMO[23] solvent continuum model (dichloromethane). Wavelength ranges of ca. 323−446 nm (**7′**) and 329−468 nm (**16′**) were covered. The UV−vis absorption spectra were simulated by using the GaussSum program.[24]

RESULTS AND DISCUSSION

Synthesis. Two tetrapalladium(II) complexes of bisazobenzene ligands (**7** and **12**) and one of an azoazoxybenzene ligand (**16**) have been prepared (Schemes 1 and 2). The symmetric dialkoxy-substituted proligand $6H_2$ was synthesized by a double diazonium coupling of TMPD with phenoxide, followed by alkylation with 1-bromo-*n*-heptane. This coupling reaction gave a very low yield, which was not improved by increasing the reaction time or by using the more powerful diazotizing agent nitrosyl sulfuric acid.

The syntheses of proligands $11H_2$ and $15H_2$ both begin with condensations of substituted nitrosoarenes with TMPD. Ethyl-4-nitrosobenzoate (**8**) was prepared by oxidizing ethyl-4-aminobenzoate with Oxone ($2KHSO_5 \cdot KHSO_4 \cdot K_2SO_4$), following an adapted literature procedure.[25] Condensing **8** with TMPD in toluene with an acetic acid catalyst yielded the azobenzene (**9**) in moderate yield (20%). Using instead acetic acid as the solvent led to self-reaction of **8** to give an asymmetric product, possibly an azoxybenzene. Diazonium coupling of **9** with phenoxide afforded the bisazobenzene **10** in moderate yield (17%). Acetic and propionic acids were used as solvents, with nitrosyl sulfuric acid as the diazotizing agent, owing to the low aqueous solubility of **9**. Reacting commercial *N*,*N*-dimethyl-4-nitrosoaniline with TMPD in acetic acid gave the unexpected azoxybenzene compound **13**. To our knowledge, the formation of an azoxybenzene

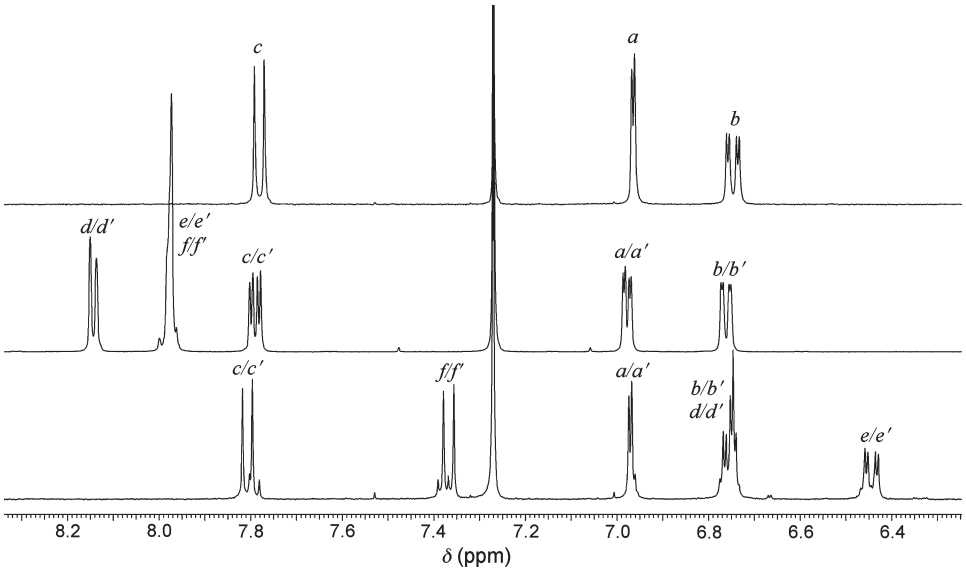

Figure 3. Aromatic regions of the ^{1}H NMR spectra of complexes **7** (top), **12** (middle), and **16** (bottom) recorded at 400 MHz in $CDCl_3$ at 293 K. See Schemes 1 and 2 for proton labels.

Table 2. UV−Vis Absorption Data for the New Proligands and Their Tetranuclear Pd^{II} Complexes in Dichloromethane[a]

terminal substituents	proligand	λ_{max}, nm (ε, 10^3 M^{-1} cm^{-1})/E_{max}, eV	complex	λ_{max}, nm (ε, 10^3 M^{-1} cm^{-1})/E_{max}, eV
OC_7H_{15}-*n*	**6H$_2$**	454 (4.2)/2.73	**7**	451 (26.0)/2.75
		345 (32.1)/3.59		380 (49.5)/3.26
				322 (43.8)/3.85
OC_7H_{15}-*n*/CO_2Et	**11H$_2$**	467 (3.7)/2.65	**12**	449 (18.9)/2.76
		350 (29.2)/3.54		381 (43.5)/3.25
				310 (50.5)/4.00
OC_7H_{15}-*n*/NMe_2	**15H$_2$**	367 (34.7)/3.38	**16**	475 (48.8)/2.61
		320 (19.5)/3.87[b]		373 (33.8)/3.32
				335 (35.4)/3.70
				300 (35.4)/4.13

[a] Solutions ca. 2×10^{-6} to 1×10^{-5} M. The ε values are the averages from measurements made at four different concentrations (with ε showing no significant concentration dependence). [b] Shoulder.

by single-step reaction of a nitrosoarene and an aniline has not been documented previously. Attempts to synthesize a symmetric bisazoxybenzene by increasing the proportion of *N*,*N*-dimethyl-4-nitrosoaniline in the reaction gave only an asymmetric product via self-reaction of the nitroso compound (as above). Nitrosoarenes often form azoxybenzenes in acidic conditions, probably via a radical mechanism.[26]

The chloride-bridged tetrapalladium complexes **7**, **12**, and **16** were synthesized by reacting the bisazobenzene and azoazoxybenzene proligands with $PdCl_2(NCPh)_2$ in refluxing ethanol. The products precipitated out in good yields (70−92%). For asymmetric ligands, a mixture of cis and trans isomers (referring to the relative orientations of ligands) was produced, as ascertained by ^{1}H NMR spectroscopy (see below). Attempts to produce analogous acetate-bridged complexes, structurally similar to reported imine-based species,[9,10] were unsuccessful. These observations may be due to steric congestion of the methyl groups as a result of the nonplanar nature of the bridging acetate ligands. To our knowledge, **16** is the first example of a mixed azobenzene/azoxybenzene chloride-bridged palladium(II) complex.

^{1}H NMR Spectroscopy. The proligands **6H$_2$**, **11H$_2$**, and **15H$_2$** all show the expected AA′BB′ signals, and the aromatic regions of the spectra of the complexes are shown in Figure 3. Signals were assigned with the aid of COSY studies where appropriate. The highly symmetric complex **7** gives three aromatic signals (Figure 3, top), a singlet due to the eight methyl groups, and one set of heptoxy signals. The signals for protons *a*−*c* shift upfield, indicating a relative shielding, on complexation of **6H$_2$**. The largest shift (0.29 ppm) occurs for proton *b*, located para with respect to the site of palladation.

The spectra of complexes **12** and **16** are more complicated than that of **7** due to lower symmetry and the presence of cis and trans isomers (Schemes 1 and 2), which give strongly overlapped signals. While **12** comprises a ca. 1:1 isomeric ratio, one isomer dominates for **16**. In dinuclear chloride-bridged palladium complexes of azobenzene ligands, the trans isomer is favored due to the differing trans effects of the C- and N-based donor sites. However, in the present complexes, the cis and trans isomers have the same arrangement of donor sites about the metal (see Crystallography below), so the distribution of isomers depends on the substituents, and the presence of the azoxy moiety in **16**.

For both **12** and **16**, the signals for the protons para to the site of palladation (*e* and *e*′) shift upfield by ca. 0.27 ppm on complexing $\mathbf{11H_2}$ and $\mathbf{15H_2}$, respectively. In **16**, the signals for the protons *f* and *f*′ shift upfield by 0.90 ppm when compared with $\mathbf{15H_2}$. This large shift may be attributable to the proximity of these protons to the azoxy oxygen (formally O^-) enforced by complexation.

Electronic Spectroscopy. The proligands $\mathbf{6H_2}$, $\mathbf{11H_2}$, and $\mathbf{15H_2}$ and complexes **7**, **12**, and **16** have been characterized by UV−vis spectroscopy in dichloromethane. The results are presented in Table 2, and representative spectra are shown in Figure 4. Note that **12** and **16** were studied as cis/trans isomeric mixtures.

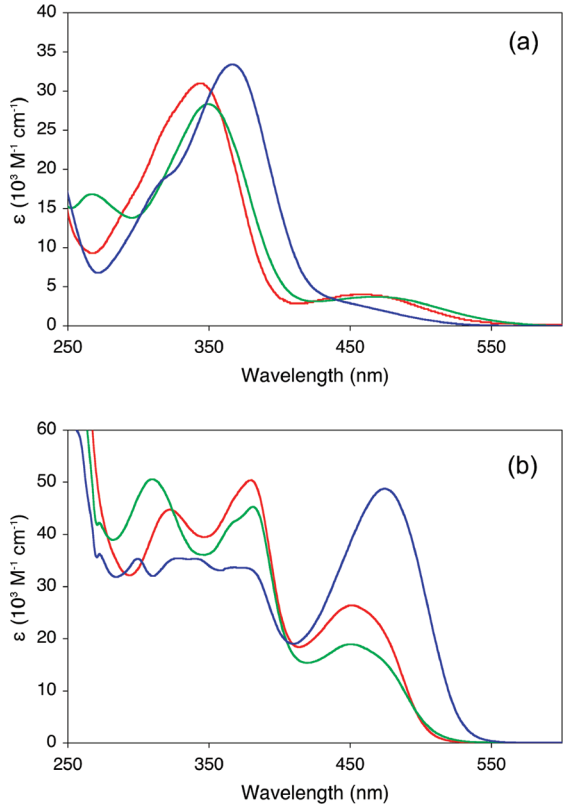

Figure 4. UV−vis absorption spectra in dichloromethane recorded at 293 K: (a) the proligands $\mathbf{6H_2}$ (red), $\mathbf{11H_2}$ (green), and $\mathbf{15H_2}$ (blue); (b) the complexes **7** (red), **12** (green), and **16** (blue).

$\mathbf{6H_2}$ and $\mathbf{11H_2}$ display intense absorption bands with respective λ_{max} values of 345 and 350 nm due to $\pi \rightarrow \pi^*$ ICT transitions (Figure 4a). In each case, a weaker band at lower energy of $n \rightarrow \pi^*$ origin is also apparent. Both bands shift bathochromically on replacing one of the heptoxy groups with $-CO_2Et$, with a larger relative change for the lower energy absorption. $\mathbf{15H_2}$ gives an intense ICT band with $\lambda_{max} = 367$ nm, but in this case the $n \rightarrow \pi^*$ transition is not resolved. The red-shift of the ICT band on moving from $\mathbf{6H_2}/\mathbf{11H_2}$ to $\mathbf{15H_2}$ is attributable to the strongly electron-donating $-NMe_2$ substituent, while the diminished intensity of the $n \rightarrow \pi^*$ transition is due to participation of n-electrons in the N−O bond.[27] The high-energy shoulder on the ICT band of $\mathbf{15H_2}$ may be ascribed to a $\pi \rightarrow \pi^*$ transition where the donor orbital involves the nitrogens and oxygen of the azoxy moiety.[28]

In acetonitrile solutions, the ICT absorption of BPAB is shifted bathochromically relative to that of (*E*)-azobenzene ($\lambda_{max} = 361$ cf. 316 nm), with an almost doubled molar extinction coefficient ($\varepsilon = 53$ cf. 29×10^3 M^{-1} cm^{-1}).[29] Matsui et al. have measured the UV−vis spectra of a large series of BPAB derivatives, almost all of which have $\lambda_{max} > 400$ nm in hexane.[12,30] Therefore, the λ_{max} and ε values for $\mathbf{6H_2}$ and $\mathbf{11H_2}$ are lower than might be expected. However, their ε values are comparable with those reported for several tetrafluoro-*p*-phenylene-centered dyes in hexane.[12] Clearly, the nonplanarity induced by the methyl substituents, as observed in the solid state for $\mathbf{6H_2}$ and $\mathbf{11H_2}$ (see below), attenuates π-conjugation, causing λ_{max} and ε to decrease.

On formation of the tetrapalladated structures, at least three bands are observed between 270 and 550 nm (Figure 4b). The spectra of **7** and **12** are similar, but that of **16** is distinctly different. This variation in optical absorption behavior is evident also in the solid state, **7** and **12** appearing dull yellow, while **16** is bright orange.

Complexes **7** and **12** both display three resolved absorption maxima, with the two higher energy bands having similar ε values and the lowest energy band being roughly half as intense. These observations contrast with the behavior of related dipalladium complexes **1**−**4** (Figure 1), for which all three bands have comparable intensities.[4] The intensities of the bands at ca. 450 nm for **7** and **12** are similar to those of **1**−**4** and diminished when compared with the ICT bands of their proligands. The latter change may be attributed to decreased coplanarity of the aryl rings on complexation. The intensities of the higher energy bands for **7** and **12** are about twice those of **1**−**4**, correlating with the number of

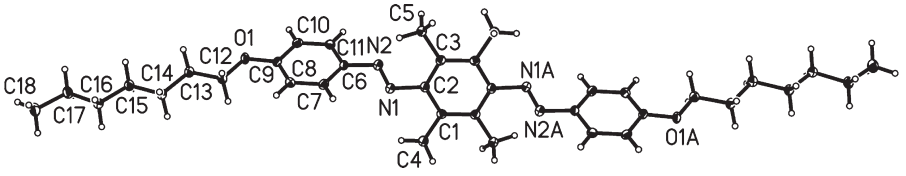

Figure 5. Representation of the molecular structure of $\mathbf{6H_2}$ (50% probability ellipsoids).

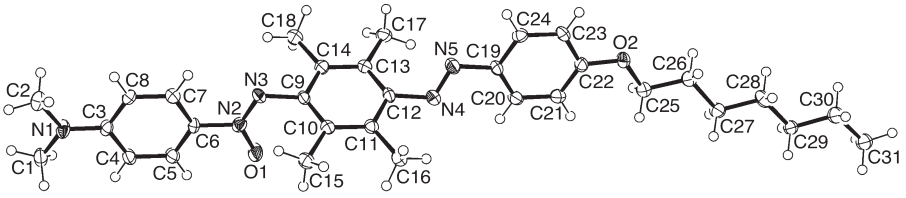

Figure 6. Representation of the molecular structure of $\mathbf{15H_2}$, with the disorder of the heptyl chain removed for clarity (50% probability ellipsoids).

dx.doi.org/10.1021/om200479g |*Organometallics* 2011, 30, 4910–4923

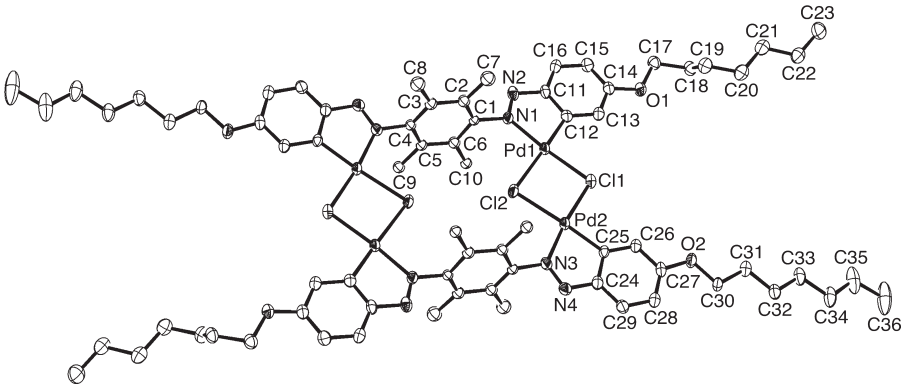

Figure 7. Representation of the molecular structure of **7**, with the disorder of the inner Cl atoms/C_6Me_4 groups and the H atoms removed for clarity (50% probability ellipsoids).

$\{Pd_2Cl_2\}^{2+}$ units. The λ_{max} values of **7** and **12** differ significantly only for the highest energy band, which is blue-shifted in **12** when compared with **7**. Slight differences in ε are also observed, and a high-energy shoulder appears on the 381 nm band of **12** (Figure 4b). These differences are attributable to lowered symmetry and the presence of isomers for **12**.

When compared with the lowest energy bands of **7** and **12**, that of complex **16** is approximately twice as intense and red-shifted. In contrast, the higher energy absorptions of **16** are less intense than those of **7** and **12**. Very little attention has been paid previously to the UV−vis spectra of cyclopalladated azoxybenzenes, but one report notes three bands (λ_{max} = 230, 329, and 433 nm in dichloromethane) for a symmetric dipalladium complex.[27]

Crystallography. Single-crystal X-ray structures have been obtained for the proligands **$6H_2$** and **$15H_2$** and complex **7**. Representations of the molecular structures are shown in Figures 5−7, and selected bond distances and angles are given in Table 3.

Only two other structures containing BPAB units have been reported,[31,32] while structures of related 1,2/1,3-isomeric compounds are more common. The structure of **$6H_2$** shows an anti conformation (Figure 5). The large dihedral angle of 72.71(8)° between the central and outer aryl rings is attributable to the steric effect of the methyl substituents. The structure of unsubstituted BPAB also shows an anti conformation, but deviates only slightly from planarity (by ca. 3°),[31] whereas the derivative Disperse Orange 29 (DO29, 1-[4-hydroxy-(*E*)-phenylazo]-4-[4-nitro-(*E*)-phenylazo]-2-methoxybenzene) adopts a syn conformation with dihedral angles of 10.9° and 14.1°.[32] The N═N bond distances in **$6H_2$** are slightly longer than those in BPAB or DO29, perhaps owing to the methyl substituents. In DO29, the N═N bond nearest to the −OMe group is elongated by ca. 0.02 Å when compared with the one on the other side of the molecule.[32]

The structure of **$15H_2$** (Figure 6) shows that the azoxy oxygen atom is bonded to the nitrogen nearest to the $-NMe_2$ group, and the terminal five carbons of the heptoxy chain are disordered over two sites. To our knowledge, this is the first crystal structure of an azoazoxybenzene. However, there are many reported structures of azoxybenzenes, including their cyclopalladated complexes,[33] and bisazoxybenzenes.[34] Zaleski and co-workers have used X-ray crystallography extensively in their studies on para-substituted azoxybenzenes.[35]

While the azo N═N bond distance in **$15H_2$** is similar to that in **$6H_2$**, the azoxy N═N distance is longer by ca. 0.02 Å; this and the N−O distance have values typical for azoxybenzenes. Also as for **$6H_2$**, **$15H_2$** shows large dihedral angles between the terminal and central aryl rings; 72.2(2)° and 74.7(2)° for the heptoxy- and $-NMe_2$-substituted rings, respectively. The slight difference in these twists

Table 3. Selected Interatomic Distances (Å) and Angles (deg) for the Proligands $6H_2$ and $15H_2$ and Complex 7

	$6H_2$	$15H_2$	7
N═N	1.260(2)	1.249(3)	1.271(5)
		1.273(3)[a]	1.274(5)
C−N	1.434(2)[b]	1.461(3)[a]	1.393(5)[c]
	1.424(2)	1.443(3)[a]	1.384(6)[c]
		1.443(3)	1.44(1)[d]
		1.437(3)	1.48(1)[d]
			1.48(1)[d]
			1.43(1)[d]
N−O		1.265(2)	
Pd−C			1.948(4)
			1.952(4)
Pd−N			1.993(4)
			1.993(4)
Pd−Cl			2.321(1)
			2.314(1)
			2.399(3)[e]
			2.507(6)[e]
			2.475(4)[e]
			2.408(4)[e]
C−N−N	113.7(1)	117.2(2)[a]	111.3(4)[c]
	113.5(1)	113.5(2)[a]	111.4(4)[c]
		113.3(2)	111.1(5)[d]
		113.6(2)	119.7(6)[d]
			111.1(5)[d]
			120.6(6)[d]
N−N−O		126.2(2)	
C−Pd−N			79.2(2)
			79.3(2)
Pd−Cl−Pd			95.75(4)
			89.7(1)[e]
			88.7(2)[e]

[a] Involving the NNO fragment. [b] Central. [c] Within the chelate rings. [d] Involving the (disordered) C_6Me_4 units. [e] Involving the inner (disordered) Cl atoms (i.e., trans to C).

dx.doi.org/10.1021/om200479g |*Organometallics* 2011, 30, 4910–4923

Table 4. Dichroic Ratios Measured in LC Hosts K15 and ZLI-2293 for UV−Vis Bands at ≥380 nm

			DR		DR	
LC	terminal substituent	proligand	380 nm	complex	380 nm	460−480 nm
K15	OC_7H_{15}-*n*	**6H$_2$**	5.3	7	2.6	4.9
ZLI-2293			6.3		2.7	5.6
K15	OC_7H_{15}-*n*/CO_2Et	**11H$_2$**	5.2	**12**	2.4	3.6
ZLI-2293			8.1		2.4	4.5
K15	OC_7H_{15}-*n*/NMe_2	**15H$_2$**	5.5	**16**	2.6	4.8
ZLI-2293			7.2		2.4	3.6

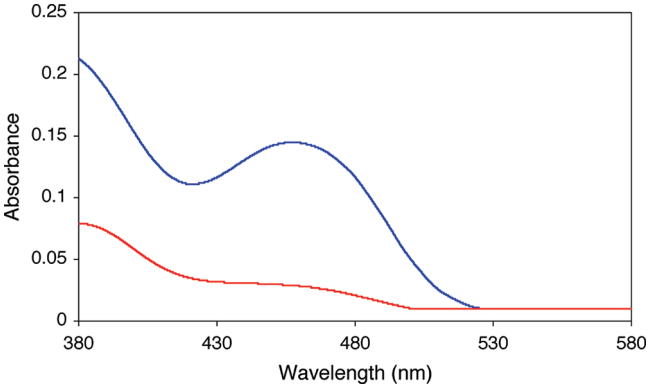

Figure 8. Electronic absorption profiles measured parallel (blue) and perpendicular (red) to the LC director for complex **7** in K15.

may be due to the presence of the azoxy oxygen atom. The NNO moiety is essentially coplanar with the $-NMe_2$-substituted ring, as is commonly observed in azoxybenzenes, possibly due to interaction of the oxygen with the adjacent ring.[35b] The $-NMe_2$ group is also almost perfectly coplanar with the adjacent ring. While the C−N(O) distance is comparable with previously reported data, the other azoxy C−N distance (1.443(3) Å) is slightly longer than corresponding literature values,[35] possibly due to the methyl groups. Deformation about the azoxy moiety, which includes an N−N−O angle of 126.2(2)°, is typically noted for azoxybenzene structures, regardless of the torsion angle of the aromatic rings.[35a,d]

The structure of **7** (Figure 7) contains an inversion center and crystallizes with one molecule of dichloromethane per Pd^{II} complex. The core of the molecule, comprising four metallocyclic units, is essentially planar. The inner chlorine atoms are disordered over two positions with unequal occupancy, forming a Cl2A−Cl1−Cl2 angle of ca. 12.0°. The central C_6Me_4 rings are also disordered over two sites unequally and form large dihedral angles with the two outer rings (ca. 74.3−88.0°). The latter angles are increased significantly with respect to the proligand **6H$_2$** due to the additional steric influence of the bridging Cl atoms. The twisting observed in **7** is comparable to, although generally larger than, that observed in the chloride-bridged dipalladium complex of 2,6-dimethyl-(*E*)-azobenzene.[36]

The azo bonds in **7** are all locked in an *E*-conformation and forced into a mutually syn arrangement. While the N=N distances do not change significantly on complexation, the C−N distances within the chelate rings shorten by ca. 0.04 Å with respect to **6H$_2$**. The bridging chlorides are forced to sit trans to two nitrogens or two carbanionic ligands, whereas in dinuclear chloride-bridged species this can be avoided with a trans arrangement of ligands.

Table 5. Selected Interatomic Distances (Å) and Angles (deg) for the Optimized (B3LYP/Def2-SVP/SDD) Structures of 7′ and 16′

	7′	16′
N=N	1.26	1.31[a]
		1.26
C−N	1.38[b]	1.42[a,b]
	1.44	1.38[b]
		1.43[a]
		1.44
N−O		1.23
Pd−C	1.98	1.98
Pd−N	2.04	2.04
		2.05[a]
Pd−Cl	2.40	2.41
	2.49[c]	2.48[c]
C−N−N	113.4[b]	114.6[a,b]
	116.5	113.3[b]
		116.7[a]
		116.6
N−N−O		123.7
C−Pd−N	78.9	80.2[a]
		78.9
Pd−Cl−Pd	95.8	96.2
	91.7[c]	92.1[c]

[a] Involving the NNO fragment. [b] Within the chelate ring. [c] For the inner Cl atoms.

The Pd−Cl distances are longer when trans to C than N (Table 3), due to the greater structural trans effect of the carbanionic ligand.[37,38] The inner Pd−Cl−Pd bond angles are therefore smaller than those to the outer Cl atoms. The Pd−C/N distances and the C−Pd−N angles are within the ranges expected for cyclopalladated complexes.[36,38] The Pd−C distances (1.948(4)/1.952(4) Å) are shorter than expected for single bonds, suggesting some multiple-bond character.[9] The intramolecular Pd···Pd separation in **7** is typical for chloride-bridged cyclopalladated complexes (3.437(1) Å) and is naturally shorter than corresponding distances in bromide/iodide-bridged tetrapalladated structures (3.662 and 3.888 Å, respectively).[9,10]

Dichroic Ratios. DR values of the proligands and complexes measured in the LCs K15 (4-pentyl-4′-cyanobiphenyl) and ZLI-2293[39] are shown in Table 4. Representative UV−vis spectra for complex **7** in K15 are shown in Figure 8. For the complexes, DRs for the two lowest energy bands were recorded. In most cases, K15 gives

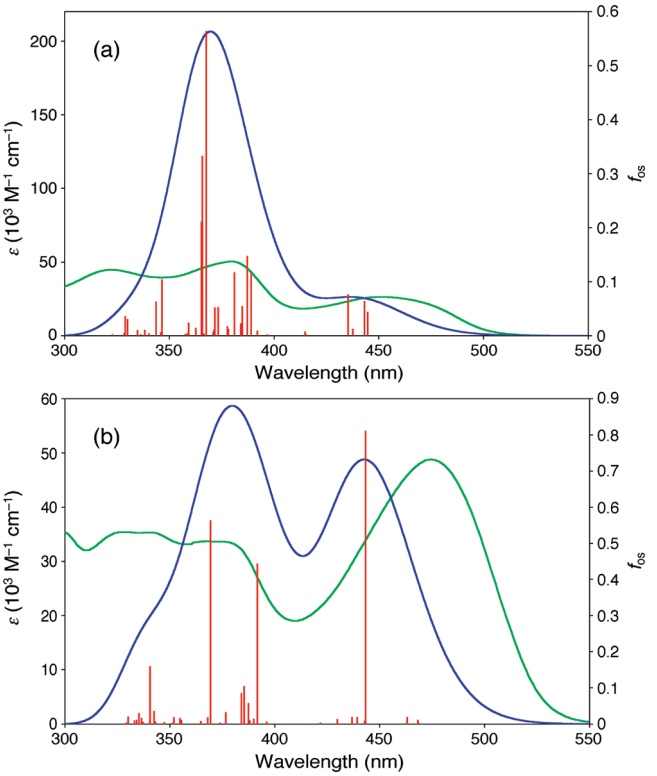

Figure 9. Respective TD-DFT-calculated (blue) and experimental (green) UV−vis spectra of (a) **7′** and **7**; (b) **16′** and **16**. The ε-axes refer to the experimental data only, and the vertical axes of the calculated data are scaled to match the main experimental absorptions. The f_{os}-axes refer to the individual calculated transitions (red).

lower DR values than ZLI-2293 since the lower clearing temperature of the former corresponds with a lower order parameter (S) at room temperature, and S generally correlates with DR.[40]

Compared with the azobenzenes we have studied previously,[4] the new bisazobenzene and azoazoxybenzene proligands do not show significantly larger DR values. Although it is established that increasing the number of azo groups enhances dichroism, adding lateral aryl substituents produces an opposite effect as the breadth of the dye increases.[11] The lower-than-expected DR values obtained for **6H$_2$**, **11H$_2$**, and **15H$_2$** are probably attributable to their twisted conformations caused by the methyl substituents.

Generally, the data for complexes **7**, **12**, and **16** are reminiscent of our studies with **1**−**4** (Figure 1), with relatively larger DR values at longer wavelengths.[4] In both LCs, the DR at 380 nm decreases distinctly on complexing **6H$_2$**, **11H$_2$**, and **15H$_2$**. Notably, the DR values of **7**, **12**, and **16** are lower than those observed for **1**−**4** at 380 nm, especially in ZLI-2293. However, when measured at 460−480 nm, both tetra- and dipalladium complexes give similar DR values. Even at these wavelengths, **7**, **12**, and **16** are still less dichroic than their proligands (although some of the differences may not be significant).

Our results imply that μ_{12} alignment with the molecular axis is most effective for the lower energy transitions of **7**, **12**, and **16**. Decreasing DR on complexation suggests less efficient ordering within the LC matrix and/or skewing of μ_{12} away from the molecular axis. It seems likely that the lack of planarity and large size of the complexes may disrupt their alignment within the LC. At 380 nm, all three complexes show very similar DRs in both

Table 6. Data from TD-DFT Calculations Based on B3LYP/Def2-SVP/SDD Geometries of Model Complexes 7′ and 16′

complex	ΔE (eV)	f_{os}	major contributions	μ_{12} (D)
7′	2.79	0.04	HOMO−1 → LUMO	2.02
			HOMO → LUMO+1	
	2.80	0.06	HOMO−6 → LUMO	2.44
			HOMO−2 → LUMO	
	2.85	0.08	HOMO−9 → LUMO+2	2.64
			HOMO−6 → LUMO	
			HOMO−1 → LUMO+3	
	3.19	0.11	HOMO−15 → LUMO+3	3.07
			HOMO−14 → LUMO	
			HOMO−10 → LUMO+1	
			HOMO−2 → LUMO	
	3.20	0.15	HOMO−10 → LUMO+4	3.47
			HOMO−7 → LUMO	
	3.25	0.12	HOMO−7 → LUMO	3.06
			HOMO−2 → LUMO+3	
			HOMO → LUMO+1	
	3.37	0.56	HOMO−9 → LUMO+2	6.63
			HOMO−4 → LUMO+1	
	3.39	0.33	HOMO−2 → LUMO	5.08
	3.39	0.21	HOMO−4 → LUMO+2	4.04
	3.58	0.10	HOMO−13 → LUMO+1	2.75
			HOMO−12 → LUMO	
			HOMO−7 → LUMO+3	
	3.61	0.06	HOMO−13 → LUMO+2	2.13
			HOMO−12 → LUMO+3	
16′	2.68	0.02	HOMO → LUMO	1.30
			HOMO → LUMO+1	
	2.80	0.81	HOMO−1 → LUMO+2	8.73
			HOMO−1 → LUMO+3	
			HOMO → LUMO+2	
			HOMO → LUMO+3	
	2.82	0.02	HOMO−10 → LUMO	1.27
			HOMO−9 → LUMO	
			HOMO−6 → LUMO+1	
			HOMO−2 → LUMO+1	
	3.16	0.44	HOMO−11 → LUMO+5	6.06
			HOMO−11 → LUMO+6	
			HOMO−10 → LUMO+4	
	3.22	0.10	HOMO−8 → LUMO+1	2.90
			HOMO−6 → LUMO+1	
	3.23	0.08	HOMO−11 → LUMO+3	2.61
			HOMO−7 → LUMO+2	
			HOMO−6 → LUMO+3	
	3.36	0.56	HOMO−8 → LUMO+1	6.64
			HOMO−5 → LUMO	
	3.64	0.16	HOMO−16 → LUMO+1	3.61
			HOMO−14 → LUMO	

LCs, while at 460−480 nm, **12** has a DR lower than those of **7** and **16** in K15. In contrast, in ZLI-2293 at 460−480 nm, the DR decreases steadily on moving along the series **7** → **12** → **16**. These observations indicate that only the shape of the central core is important and that the μ_{12} directions are similar for analogous

dx.doi.org/10.1021/om200479g |*Organometallics* 2011, 30, 4910–4923

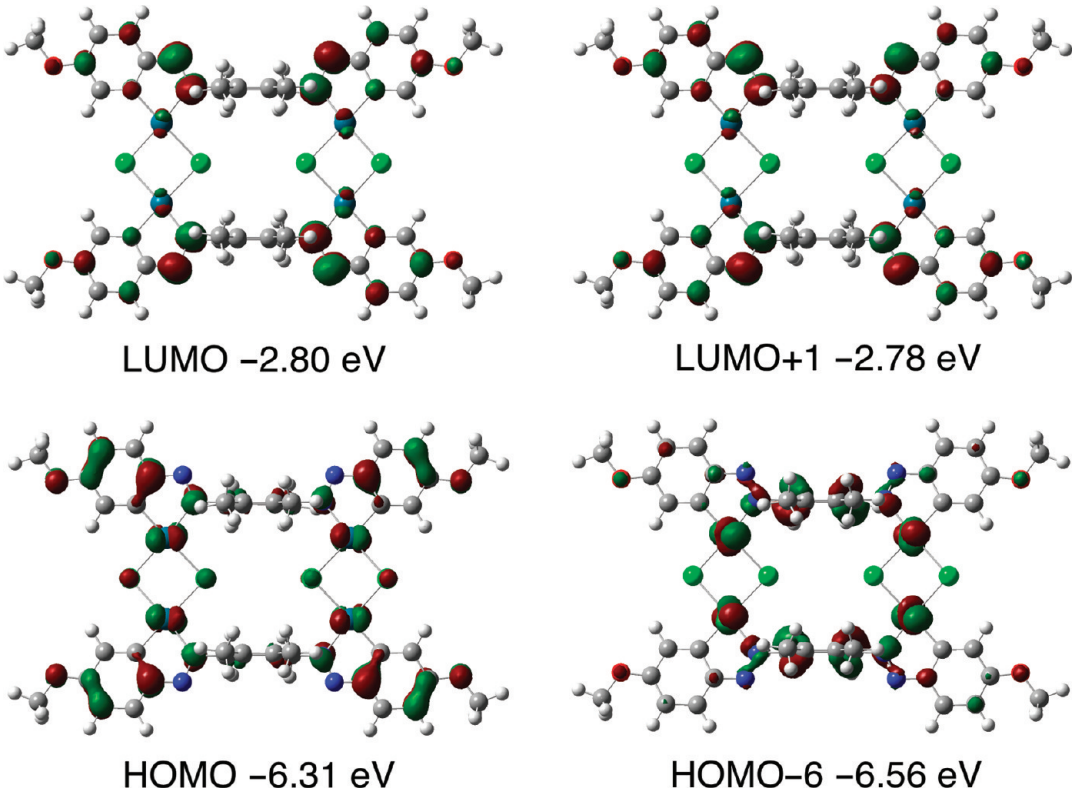

Figure 10. TD-DFT-derived pictures of orbitals involved in transitions associated with the low-energy absorption band of 7′ (isosurface value 0.03 au).

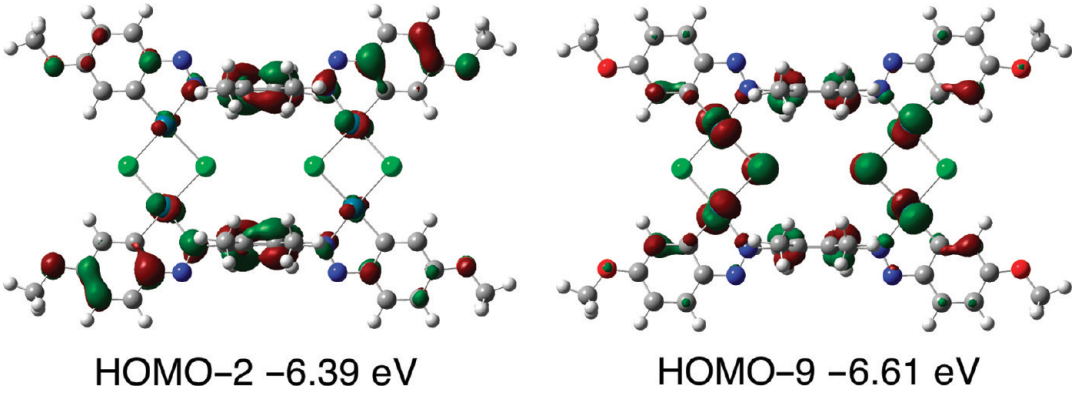

Figure 11. TD-DFT-derived pictures of HOMOs involved in higher energy transitions of 7′ (isosurface value 0.03 au).

bands, when measuring at 380 nm. However, replacing two of the heptoxy chains with $-CO_2Et$ or $-NMe_2$ substituents does affect the dichroic behavior at longer wavelengths.

Theoretical Studies. In order to rationalize the measured UV−vis and DR data, TD-DFT calculations were carried out on the methoxy analogues (denoted 7′ and **16**′) of complexes **7** and **16** by using Gaussian 03.[22] For **16**′, only the trans isomer is considered.

Selected optimized bond distances and angles are given in Table 5. Comparison of the crystallographic data for **7** with the optimized geometry of 7′ shows reasonable agreement, the largest discrepancies being +0.09 Å (Pd−Cl) and ca. +3° (Pd−Cl−Pd). However, the optimized structure is more distorted with a bend about the Cl···Cl axis of 12.41° and dihedral angles between the central and outer rings of 85.47° and 82.42°. The optimized geometry of **16**′ resembles that of 7′. The relative extension of the azoxy compared with the azo N=N distance, observed crystallographically for **15H$_2$**, also occurs in **16**′. A 11.82° departure from planarity and dihedral angles between the central and outer rings of 87.36° and 75.61° are predicted for **16**′.

The UV−vis spectra for 7′ and **16**′ simulated by using GaussSum[24] are shown in Figure 9, with the experimental spectra of **7** and **16**. Predicted transition energies are presented in Table 6 and MOs involved in major transitions are depicted in Figures 10−13. The lowest energy bands are blue-shifted with respect to the experimental spectra, especially for **16**′. Multiple transitions contribute to this band for 7′, while in **16**′ one transition dominates. **16**′ also shows fewer significant transitions at higher

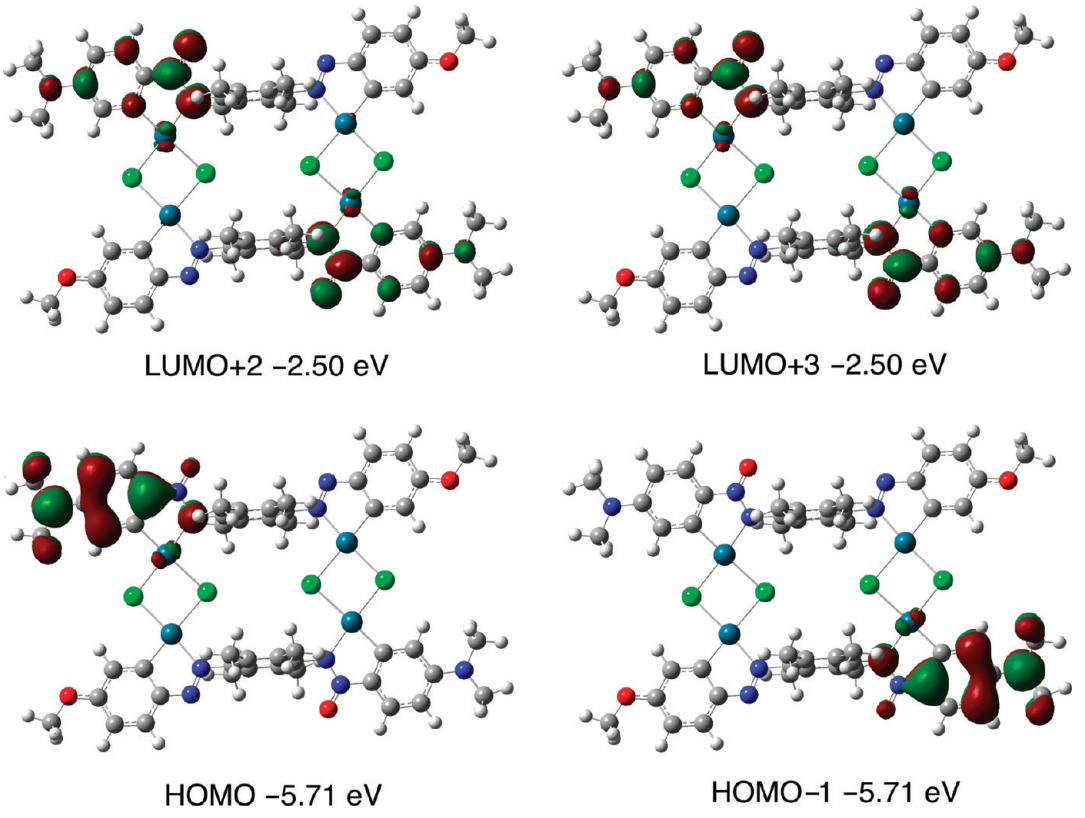

Figure 12. TD-DFT-derived pictures of orbitals associated with the transition at ΔE = 2.80 eV for **16′** (isosurface value 0.03 au).

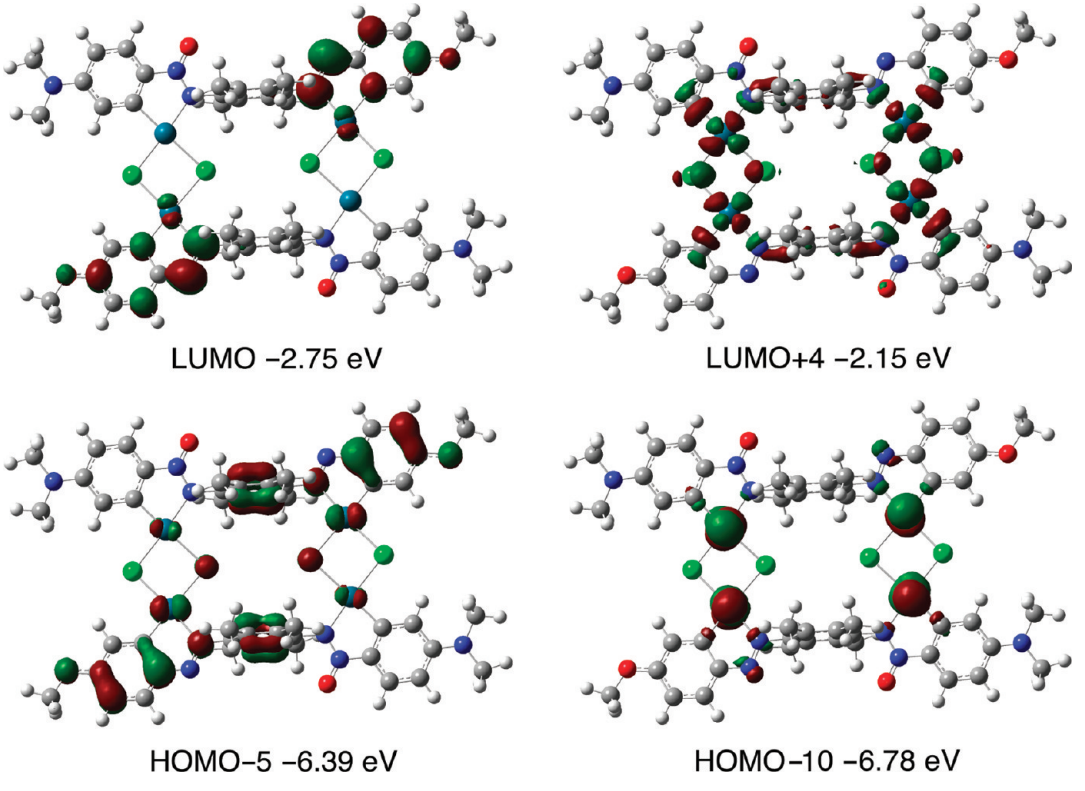

Figure 13. TD-DFT-derived pictures of selected orbitals associated with the higher energy transitions of **16′** (isosurface value 0.03 au).

dx.doi.org/10.1021/om200479g |*Organometallics* 2011, 30, 4910–4923

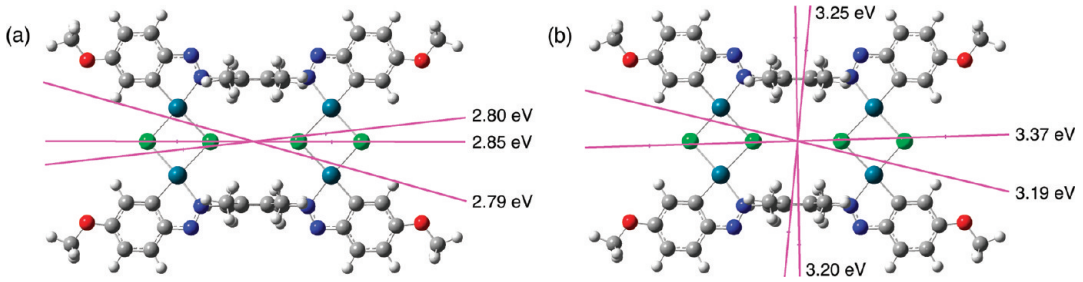

Figure 14. Calculated μ_{12} vectors (scaled to show direction) of **7′** for transitions at (a) low energy and (b) high energy.

energies when compared with **7′**. In both cases, the predicted absorption profiles do not match well with those observed, although the presence of isomers of **16** is ignored in the calculations. For **7′**, the discrepancy between the relative intensities of low- and high-energy bands is large, as also noted in our previous studies with dinuclear complexes.[4] However, the oscillator strengths f_{os} of the predicted transitions correlate with the observed doubly intense low-energy band for **16** when compared with **7**. Three transitions with $f_{os} < 0.1$ form this band in **7′**, while the major low-energy transition in **16′** has $f_{os} = 0.81$.

For the low-energy band of **7′**, the HOMOs involve the BPAB ligands, metals, and chloride bridges, while the LUMOs are primarily different phase combinations of BPAB π^* orbitals (Figure 10). These results contrast with those for related dinuclear species, for which this band involves almost exclusively azobenzene-based transitions.[4] The break in conjugation caused by the twisted central rings influences the nature of the contributing MOs in **7′**. The orbitals involved in the higher energy transitions show distributions similar to those mentioned above, with the HOMOs showing contributions from all over the complex (Figure 11).

The orbital origins of the lowest energy band of **16′** contrast with those of **7′**. The dominant transition at ΔE = 2.80 eV involves the orbitals shown in Figure 12 where the degenerate pairs HOMO/HOMO−1 and LUMO+2/LUMO+3 are located on the cyclopalladated N═N(O)$C_6H_3NMe_2$ units. This transition has charge-transfer character (from amino donor to azoxy acceptor) and accounts for the differences observed in the low-energy region of the electronic spectra of **7**/**12** and **16**. Two transitions are dominant at higher energy; selected orbitals involved are shown in Figure 13.

The μ_{12} directions have been approximated for the major calculated transitions. For **7′**, the μ_{12} vectors of the two dominant low-energy transitions align well with the long molecular axis, while the lowest energy transition (ΔE = 2.79 eV) shows a moderate degree of alignment. (Figure 14a). At higher energies, some transitions retain good alignment, while others show perpendicular μ_{12} vectors (Figure 14b). The lowest energy transition with substantial intensity (ΔE = 2.80 eV) of **16′** also shows good axial alignment of μ_{12}, with poorer alignment at higher energies (see Supporting Information, Figure S1). These results correlate broadly with the observed relatively higher DR values for the low-energy bands.

CONCLUSION

New BPAB derivatives and an azoazoxybenzene have been cyclopalladated to yield new chloride-bridged tetranuclear palladium(II) complexes with a rectangular motif, using methyl groups to block unwanted palladation. Reaction between *N*,*N*-dimethyl-4-nitrosoaniline and TMPD in acidic conditions yielded an unexpected azoxybenzene precursor. ^{1}H NMR spectra reveal that mixtures of cis and trans isomers are formed with asymmetric ligands. Single-crystal X-ray structures of two proligands and one complex show that the methyl groups on the central aryl rings cause severe departures from planarity, especially in the complex, where the chloride bridges provide additional steric hindrance. UV−vis spectra are also influenced by the structural distortions, decreased conjugation resulting in lower-than-expected $\pi \rightarrow \pi^*$ transition intensities. While the BPAB complexes give quite similar spectra, the azoazoxybenzene complex displays a doubly intense low-energy transition. The results of DR measurements are reminiscent of those for related dinuclear azobenzene complexes, with complexation proving unbeneficial. Relatively poor alignment within the LC may result from the bulky shape of the complexes. The DR values of the low-energy bands are larger than those determined at higher energies. TD-DFT calculations reveal that the origins of the low-energy transitions differ for BPAB and azoazoxybenzene complexes, the latter involving charge transfer from the $C_6H_3NMe_2$ groups, explaining the observed spectral differences. The origin of the low-energy transition of the BPAB complex is also quite different from that in the related dinuclear complexes. The directions of the μ_{12} vectors with respect to the long molecular axes generally correlate with the observed DR values, since alignment is best for the low-energy transitions.

ASSOCIATED CONTENT

Supporting Information. Crystallographic information in CIF format; Cartesian coordinates of theoretically optimized geometries for **7′** and **16′**; calculated μ_{12} vectors of **16′**. This material is available free of charge via the Internet at http://pubs.acs.org.

AUTHOR INFORMATION

Corresponding Author
*E-mail: b.coe@manchester.ac.uk.

ACKNOWLEDGMENT

We thank DyStar U.K. Ltd and the University of Manchester for support. We are grateful to Dr. Michael G. Hutchings (DyStar) for initiating this project and also to Dr. Joseph J. W. McDouall (Manchester) for advice concerning TD-DFT calculations. Dr. Robin G. Pritchard (Manchester) is also gratefully acknowledged for rerefining two of the X-ray crystal structures. Hewlett-Packard Ltd are thanked for the use of the dichrometer and generous donations of LCs.

REFERENCES

(1) (a) Herrmann, W. A.; Böhm, V. P. W.; Reisinger, C.-P. *J. Organomet. Chem.* **1999**, *576*, 23. (b) Dupont, J.; Pfeffer, M.; Spencer, J. *Eur. J. Inorg. Chem.* **2001**, 1917. (c) Beletskaya, I. P.; Cheprakov, A. V. *J. Organomet. Chem.* **2004**, *689*, 4055. (d) Dupont, J.; Consorti, C. S.; Spencer, J. *Chem. Rev.* **2005**, *105*, 2527.

(2) (a) Buey, J.; Coco, S.; Díez, L.; Espinet, P.; Martín-Alvarez, J. M.; Miguel, J. A. *Organometallics* **1998**, *17*, 1750. (b) Aiello, I.; Dattilo, D.; Ghedini, M.; Golemme, A. *J. Am. Chem. Soc.* **2001**, *123*, 5598. (c) Aiello, I.; Dattilo, D.; Ghedini, M.; Bruno, A.; Termine, R.; Golemme, A. *Adv. Mater.* **2002**, *14*, 1233. (d) Termine, R.; Talarico, M.; Aiello, I.; Dattilo, D.; Pucci, D.; Ghedini, M.; Golemme, A. *Opto-Electron. Rev.* **2005**, *13*, 287. (e) Espinet, P.; Miguel, J. A.; Martín-Alvarez, J. M.; Villacampa, B. *J. Organomet. Chem.* **2010**, *695*, 437.

(3) Ghedini, M.; Aiello, I.; Crispini, A.; Golemme, A.; La Deda, M.; Pucci, D. *Coord. Chem. Rev.* **2006**, *250*, 1373. (b) Buey, J.; Espinet, P. *J. Organomet. Chem.* **1996**, *507*, 137.

(4) Blackburn, O. A.; Coe, B. J. *Organometallics* **2011**, *30*, 2212.

(5) (a) Marshall, K. L.; Painter, G.; Lotito, K.; Noto, A. G.; Chang, P. *Mol. Cryst. Liq. Cryst.* **2006**, *454*, 47. (b) Bruce, D. W.; Dunmur, D. A.; Hunt, S. E.; Maitlis, P. M.; Orr, R. *J. Mater. Chem.* **1991**, *1*, 857.

(6) Blackburn, O. A.; Coe, B. J.; Fielden, J.; Helliwell, M.; McDouall, J. J. W.; Hutchings, M. G. *Inorg. Chem.* **2010**, *49*, 9136.

(7) (a) Heilmeier, G. H.; Zanoni, L. A. *Appl. Phys. Lett.* **1968**, *13*, 91. (b) White, D. L.; Taylor, G. N. *J. Appl. Phys.* **1974**, *45*, 4718.

(8) (a) Harris, S. *Nat. Photonics* **2010**, *4*, 748. (b) Sobel, A. *Nat. Mater.* **2003**, *2*, 643. (c) Graham-Rowe, D. *Nat. Photonics* **2007**, *1*, 248.

(9) Vila, J. M.; Gayoso, M.; Pereira, M. T.; Rodriguez, M. C.; Ortigueira, J. M.; Thornton-Pett, M. *J. Organomet. Chem.* **1992**, *426*, 267.

(10) Praefcke, K.; Diele, S.; Pickardt, J.; Gündoğan, B.; Nütz, U.; Singer, D. *Liq. Cryst.* **1995**, *18*, 857.

(11) (a) Bahadur, B.; Sarna, R. K.; Bhide, V. G. *Mol. Cryst. Liq. Cryst.* **1981**, *75*, 121. (b) Bloom, A.; Hung, P. L. K. *Mol. Cryst. Liq. Cryst.* **1977**, *40*, 213. (c) Constant, J.; Raynes, E. P.; Shanks, I. A.; Coates, D.; Gray, G. W.; McDonnell, D. G. *J. Phys. D: Appl. Phys.* **1978**, *11*, 479.

(12) Matsui, M.; Tanaka, N.; Andoh, N.; Funabiki, K.; Shibata, K.; Muramatsu, H.; Ishigure, Y.; Kohyama, E.; Abe, Y.; Kaneko, M. *Chem. Mater.* **1998**, *10*, 1921.

(13) Robin, M. B.; Simpson, W. T. *J. Chem. Phys.* **1962**, *36*, 580.

(14) Fan, G.-Z.; Li, T.; Li, G.-X. *Appl. Organomet. Chem.* **2006**, *20*, 656.

(15) *SAINT* (Version 6.45); Bruker AXS Inc.: Madison, WI, USA, 2003.

(16) *SADABS* (Version 2.10); Bruker AXS Inc.: Madison, WI, USA, 2003.

(17) Sheldrick, G. M. *Acta Crystallogr., Sect. A* **1990**, *46*, 467.

(18) Sheldrick, G. M. *SHELXS 97, Programs for Crystal Structure Analysis* (Release 97-2); University of Göttingen: Göttingen, Germany, 1997.

(19) Becke, A. D. *J. Chem. Phys.* **1993**, *98*, 5648.

(20) Weigend, F.; Ahlrichs, R. *Phys. Chem. Chem. Phys.* **2005**, *7*, 3297.

(21) Andrae, D.; Häussermann, U.; Dolg, M.; Stoll, H.; Preuss, H. *Theor. Chim. Acta* **1990**, *77*, 123.

(22) Frisch, M. J.; Trucks, G. W.; Schlegel, H. B.; Scuseria, G. E.; Robb, M. A.; Cheeseman, V. G.; Montgomery, J. A., Vreven, Jr. T.; Kudin, K. N.; Burant, J. C.; Millam, J. M.; Iyengar, S. S.; Tomasi, J.; Barone, V.; Mennucci, B.; Cossi, M.; Scalmani, G.; Rega, N.; Petersson, G. A.; Nakatsuji, H.; Hada, M.; Ehara, M.; Toyota, K.; Fukuda, R.; Hasegawa, J.; Ishida, M.; Nakajima, T.; Honda, Y.; Kitao, O.; Nakai, H.; Klene, M.; Li, X.; Knox, J. E.; Hratchian, H. P.; Cross, J. B.; Adamo, C.; Jaramillo, J.; Gomperts, R.; Stratmann, R. E.; Yazyev, O.; Austin, A. J.; Cammi, R.; Pomelli, C.; Ochterski, J. W.; Ayala, P. Y.; Morokuma, K.; Voth, G. A.; Salvador, P.; Dannenberg, J. J.; Zakrzewski, V. G.; Dapprich, S.; Daniels, A. D.; Strain, M. C.; Farkas, O.; Malick, D. K.; Rabuck, A. D.; Raghavachari, K.; Foresman, J. B.; Ortiz, J. V.; Cui, Q.; Baboul, A. G.; Clifford, S.; Cioslowski, J.; Stefanov, B. B.; Liu, G.; Liashenko, A.; Piskorz, P.; Komaromi, I.; Martin, R. L.; Fox, D. J.; Keith, T.; Al-Laham, M. A.; Peng, C. Y.; Nanayakkara, A.; Challacombe, M.; Gill, P. M. W.; Johnson, B.; Chen, W.; Wong, M. W.; Gonzalez, C.; Pople, J. A. *Gaussian 03*, Revision C.02; Gaussian, Inc.: Wallingford, CT, 2004.

(23) Eckert, F.; Klamt, A. *AIChE J.* **2002**, *48*, 369.

(24) O'Boyle, N. M.; Tenderholt, A. L.; Langner, K. M. *J. Comput. Chem.* **2008**, *29*, 839.

(25) Priewisch, B.; Rück-Braun, K. *J. Org. Chem.* **2005**, *70*, 2350.

(26) Cardellini, L.; Carloni, P.; Damiani, E.; Greci, L.; Stipa, P.; Rizzoli, C.; Sgarabotto, P. *J. Chem. Soc., Perkin Trans. 2* **1994**, 1589.

(27) Ghedini, M.; Pucci, D.; Crispini, A; Aiello, I.; Barigelletti, F.; Gessi, A.; Francescangeli, O. *Appl. Organomet. Chem.* **1999**, *13*, 565.

(28) (a) Tosi, C. *Spectrochim. Acta* **1966**, *22*, 1701. (b) Gore, P. H.; Wheeler, O. H. *J. Am. Chem. Soc.* **1956**, *78*, 2160.

(29) Cisnetti, F.; Ballardini, R.; Credi, A.; Gandolfi, M. T.; Masiero, S.; Negri, F.; Pieraccini, S.; Spada, G. P. *Chem.—Eur. J.* **2004**, *10*, 2011.

(30) Matsui, M.; Nakagawa, H.; Joglekar, B.; Shibata, K.; Muramatsu, H.; Abe, Y.; Kaneko, M. *Liq. Cryst.* **1996**, *21*, 669.

(31) Gilardi, R. D.; Karle, I. L. *Acta Crystallogr., Sect. B* **1972**, *28*, 1635.

(32) Freeman, H. S.; McIntosh, S. A.; Singh, P. *Dyes Pigments* **1997**, *35*, 11.

(33) Ghedini, M.; Morrone, S.; De Munno, G.; Crispini, A. *J. Organomet. Chem.* **1991**, *415*, 281.

(34) Wakahara, A.; Fujiwara, T.; Ikeda, M.; Tamura, Y.; Tomita, K.-I. *Acta Crystallogr. Sect. C* **1983**, *39*, 99.

(35) (a) Ejsmont, K.; Domański, A.; Kyzioł, J. B.; Zaleski, J. *Acta Crystallogr. Sect. C* **2000**, *56*, 697. (b) Domański, A.; Ejsmont, K.; Kyzioł, J. B.; Zaleski, J. *Acta Crystallogr. Sect. C* **2001**, *57*, 467. (c) Ejsmont, K.; Domański, A.; Kyzioł, J. B.; Zaleski, J. *Acta Crystallogr. Sect. C* **2004**, *60*, o368. (d) Ejsmont, K.; Domański, A.; Kyzioł, J. B.; Zaleski, J. *J. Mol. Struct.* **2005**, *753*, 92.

(36) Armentano, S.; Crispini, A.; De Munno, G.; Ghedini, M.; Neve, F. *Acta Crystallogr. Sect. C* **1991**, *47*, 966.

(37) Barr, N.; Dyke, S. F.; Smith, G.; Kennard, C. H. L.; McKee, V. *J. Organomet. Chem.* **1985**, *288*, 109.

(38) Armentano, S.; Crispini, A.; De Munno, G.; Ghedini, M.; Neve, F. *Acta Crystallogr. Sect. C* **1991**, *47*, 2545.

(39) The precise composition of ZLI-2293 is unknown to us. However, ^{1}H NMR spectroscopy obtained in $CDCl_3$ reveals it to contain primarily 4,4′-disubstituted cyclohexylbenzene derivatives with long alkyl chains.

(40) (a) Ichinose, H.; Sato, H.; Naemura, S. *Mol. Cryst. Liq. Cryst.* **2004**, *409*, 401. (b) Cognard, J.; Phan, T. H. *Mol. Cryst. Liq. Cryst.* **1981**, *68*, 207.